Translated from *Uspekhi Khimii*, **56**, 1639-1658 (1987) U.D.C. 539.18; 577.323

Mössbauer Studies of Tunnel Phenomena in Chemical and Biological Physics

V.I.Gol'danskii

The combination of various methods based on the use of the Mössbauer effect, namely the traditional Mössbauer absorption spectroscopy, Mössbauer emission spectroscopy, and the Rayleigh scattering of Mössbauer emission, has made it possible to observe a series of characteristic features of the kinetics of intramolecular oxidation-reduction processes (in relation to the conversion of Turnbull's blue into Prussian blue) and to investigate the dynamic properties of biopolymers over a wide range of temperatures and degrees of hydration.
A very important role of tunnel processes was discovered in both cases—the intramolecular tunnel electron transfer (electronic-nuclear tunnelling) and the phonon-stimulated tunnelling of atoms and atomic groups respectively.
The bibliography includes 75 references.

CONTENTS

I. Introduction 935
II. Studies of the intramolecular tunnel electron transfer by the MES method 935
III. Studies of the dynamic properties of biopolymers by the RSME method 940

I. INTRODUCTION

A characteristic feature of the current employment of isotopes in various natural sciences is the fact that not only the radioactivity itself but also the properties of the radioactive decomposition (its rate and mechanism) and of the radiation emitted (energy and hyperfine spectra, absorption and scattering, angular correlations etc.) serve as sources of physicochemical information.

Many types of transformations of atomic nuclei and elementary particles are known (they are listed in Table 1), in which various effects of the atomic, molecular, and crystal environment are manifested and all the effects can be used to study this environment, especially its structural and dynamic properties.

Table 1. The transformations of atomic nuclei and elementary particles observed with the aid of radioisotopes and the effects of the atomic, molecular, and crystalline environments manifested in such observations.

Transformation	Effect
Electron capture	Changes in lifetime
Isomeric transitions (with internal electronic conversion)	Changes in conversion coefficients and lifetime
Mössbauer isomeric transitions	Changes in structural and dynamic parameters of Mössbauer spectra
Cascade transitions ($\gamma\gamma$, $\beta\gamma$, etc)	Perturbation of angular correlations
Emission of γ-rays or particles by polarised nuclei	Perturbation of the angular distribution of the emitted γ-rays or particles relative to the direction of spin
Annihilation of positrons	Changes in the lifetime of positrons and of the number and the angular and energy correlations of the annihilated γ-quanta

Two phenomena in the physics of atomic nuclear and elementary particles where the influence of the properties of the environment—the Mössbauer effect and the annihilation of slow positrons—are strikingly observed, have been particularly vigorously investigated by the Structure of Matter Division of the Institute of Chemical Physics at the USSR Academy of Sciences.[1-4] A wide range of our investigations has been devoted to the development and application of chemical Mössbauer spectroscopy (MS). We began with the most traditional method—Mössbauer absorption spectroscopy (MAS), but subsequently the range of methods employed was extended and included also Mössbauer emission spectroscopy (MES), the Mössbauer spectroscopy of conversion electrons (MSCE), and the Rayleigh scattering of the Mössbauer emission (RSME).

In the present review we shall consider the application of MES and RSME to the study of tunnel phenomena in chemical and biological physics, namely the intramolecular tunnel electron transfer and the phonon-stimulated tunnelling of atoms and atomic groups in biopolymers. Thus we proceed from two directions—we apply various Mössbauer methods (MES and RSME in combination with MAS), investigate various objects, sometimes widely differing in their nature, namely inorganic coordination compounds and bio-organic macromolecules. Nevertheless the results obtained are closely related and supplement one another; they all deepen and extend our understanding of tunnelling processes and thus fall within the general range of studies of the tunnel effect in chemistry, electronic-nuclear and molecular tunnelling, and the low-temperature quantum limit of the rates of chemical reactions.[5-8]

II. STUDIES OF THE INTRAMOLECULAR TUNNEL ELECTRON TRANSFER BY THE MES METHOD

We shall begin with the use of Mössbauer spectroscopy (MES and MAS) in the study of the spatial and time delocalisation of electrons in molecules or more complex systems.[9] It is evident that, if we are dealing with a system of two potential wells separated by a barrier (Fig.1), then the electronic levels located above this barrier belong to neither the left-hand nor to the right-hand well and describe the system as a whole. For the sub-barrier levels, the situation is more complex.

We shall consider, for example, the simplest case of the behaviour of the electron in two identical potential wells, where it occupies one of the sub-barrier levels. It can be seen that in this case one could assume that the electron

is either in the left-hand well (wave function ψ_l) or in the right-hand well (wave function ψ_r). However, neither of these positions of the electron (i.e. its spatial localisation) corresponds to the eigenstate of such a system. The eigenstates are symmetric $\psi_s = (1/\sqrt{2})(\psi_l + \psi_r)$ or antisymmetric $\psi_a = (1/\sqrt{2})(\psi_l - \psi_r)$ combinations of the wave functions ψ_l and ψ_r with energies differing by $\Delta E_{as} = \hbar/\tau$.

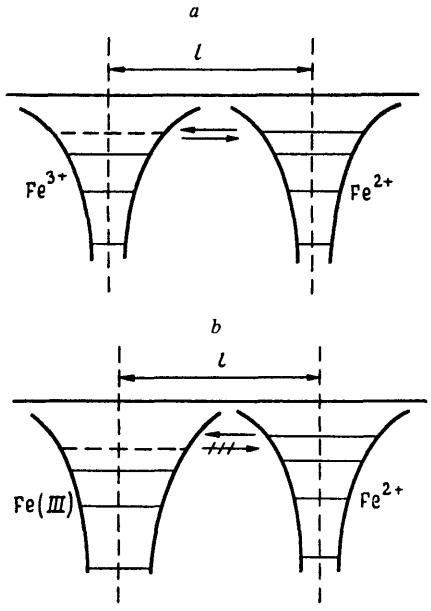


Figure 1. Schematic illustration of the spatial and time delocalisation of electrons in systems with two potential wells: *a*) two potential wells (to the left and to the right); the systems of their electronic levels are the same and correspond to high-spin iron; the electron jump from Fe^{2+} to Fe^{3+}, indicated by an arrow, can take place in either direction (spatial delocalisation of the electron); *b*) two potential wells; the systems of their electronic levels are different—the low-spin state of iron on the left and the high-spin state of iron on the right; the spontaneous electron transition from the upper level can take place only from right to left.

The energy splitting is thus related to the characteristic localisation time τ or, in other words, to the time required for the oscillation (jump) of the electron between the left-hand and right-hand wells. Only if the time τ is large compared with the characteristic time of the measurement by the given experimental method (τ_{exp}) is it possible to observe the spatial localisation of the states ψ_l and ψ_r.

For example, if the electron is in a system where two identical potential wells are represented by two high-spin tervalent iron ions Fe^{3+} (the ions *a* and *b*) then the wave function ψ_l will describe the Fe_a^{2+}–Fe_b^{3+} state, while the wave function ψ_r will describe the Fe_a^{3+}–Fe_b^{2+} state (Fig.1*a*). Each of these ions (*a* and *b*) spends 50% of time in the high-spin states of bivalent iron (Fe^{2+}) and tervalent iron (Fe^{3+}). The characteristic time of the measurement in Mössbauer spectroscopy is the average lifetime of the excited level $\tau_{exp} = \tau_M$, which is $\tau_M = 1.4 \times 10^{-7}$ s for ^{57}Fe. It the time taken for the electron jump between the two wells is greater than or comparable to the lifetime, $\tau \gtrsim \tau_M$, then two Mössbauer absorption spectra, representing both Fe^{2+} and Fe^{3+}, will be observed. If the jump time is much shorter than the time of the Mössbauer transition, $\tau \ll \tau_M$, only one Mössbauer spectrum, intermediate between those of Fe^{2+} and Fe^{3+}, will be observed. Thus MAS makes it possible not only to establish the very fact of the spatial delocalisation of electrons but also to investigate quantitatively the time scale characterising the electron jumps between different states.

The use of MES opens up new possibilities. Suppose that there are two different potential wells, for example, two tervalent iron ions, differing in their properties: we shall assume that one of them is in the high-spin (Fe^{3+}) state and the other is in the low-spin [Fe(III)] state (Fig.1*b*). In this case the presence of an additional electron in one of these potential wells is energetically more favourable than its presence in the other well and for this reason only one of the two possible states—the one with the lower energy—is represented in the usual (absorption) Mössbauer spectra.

However, we shall assume that at the instant of the formation of the Mössbauer nuclear level, the corresponding atom is in a higher, unstable electronic state of the system and that the system passes to a stable state only later, while the characteristic time of the transition is close to or greater than the lifetime of the Mössbauer level. In this case there is a possibility of noting the contribution of the initial unstable state of the system to the Mössbauer emission spectrum. This contribution may be especially significant for short time intervals immediately after the population of the Mössbauer level.

All these general considerations can be clearly illustrated in relation to compounds well known to chemists—the ferricyanide–ferrocyanide complexes called Prussian blue (PB) and Turnbull's blue (TB). The formation of these beautiful blue deposits is used to detect the high-spin Fe^{3+} or Fe^{2+} ions in solutions. The addition of potassium ferrocyanide $K_4[Fe^{II}(CN)_6]$, a salt of the low-spin bivalent iron, to Fe^{3+} salts causes the precipitation of PB, tentatively having the composition $Fe_4^{3+}[Fe^{II}(CN)_6]_3^{4-}$, while the addition of potassium ferricyanide $K_3[Fe^{III}(CN)_6]$. a salt of the low-spin tervalent iron, to Fe^{2+} salts leads to the formation of TB, which has the tentative composition $Fe_3^{2+}[Fe^{III}(CN)_6]_2^{3-}$.

All four forms of iron participating in these reactions—Fe^{3+}, Fe^{2+}, Fe(III), and Fe(II)—have different Mössbauer spectra (Fig.2); it is therefore not surprising that already in the very earliest stage of development of Mössbauer spectroscopy several laboratories in different countries (including our laboratory) began to investigate the absorption spectra of PB and TB in an attempt to identify both compounds. However, it was found that, whatever method used to prepare the compounds (Fig.2), only one resultant spectrum was always obtained, i.e. only one product, namely PB whose structure is illustrated in Fig.3, with low-spin bivalent iron Fe(II) ions adjoining carbon atoms, i.e. in an environment of ligands with a strong field, and high-spin tervalent iron (Fe^{3+}) ions adjoining nitrogen atoms, i.e. in an environment of ligands with a weak field; the additional Fe^{3+} ions occupy interstitial positions. The impression was created that TB does not exist at all and that the electron is always localised (in conformity with the situation illustrated in Fig.1*b*) at low-spin iron in all ferri-ferrocyanides.

The formation of precisely PB and not TB in all the procedures, listed above, for the preparation of iron cyanide complexes can be seen particularly clearly when the Mössbauer effect is used to analyse the position of the isotope label[10]—a method which is extremely convenient for the study

of the structures, kinetics, and mechanisms of reactions of systems containing Mössbauer atoms in different functional states. In the instances described, the application of the Mössbauer effect involved the comparison of the absorption spectra with selective introduction of ^{57}Fe labels in the form of one of the four states of iron in one or both interacting compounds.[11]

Apart from the fact that the employment of the Mössbauer effect to analyse the state of the isotope labels confirmed the formation of Prussian blue and not Turnbull's blue in all the instances investigated, it also demonstrated that the sequence of the formation of the soluble and insoluble ferri-ferrocyanides differs significantly from, and sometimes is even completely opposed to, that adopted in the literature and that isotope exchange took place in solutions between different states of iron. However, these problems will not be discussed here and we shall proceed to experiments on Mössbauer emission spectroscopy (MES).

MES characterises the structural and dynamic properties of compounds containing emitters of resonance γ-quanta, i.e. atoms or nuclei in the highest excited Mössbauer level. The possibilities for the study of relaxation changes in such compounds are determined by the ratio of the lifetime of the Mössbauer level τ_M to the characteristic relaxation time τ_r. When $\tau_r \ll \tau_M$, relaxation takes place mainly before the nuclear transition and the emission spectra integrated with respect to time (IMES) therefore reflect principally the properties of emitters which have not undergone relaxation.

Nevertheless the use of delayed coincidences schemes with resolution time $\tau_{coinc} < \tau_M$, i.e. the study of the emission spectra differentiated with respect to time (DMES), leads to additional possibilities for the investigation of rapid relaxation processes. When $\tau_r \gg \tau_M$, predominantly atoms with unexcited nuclei, in the ground state, participate in the relaxation process and MES does not therefore carry any additional information.

Consequently the most favourable condition for the application of MES in its simplest (IMES) version is $\tau_r \sim \tau_M$. The usual values of τ_M are in the range 10^{-5}–10^{-10} s, while for ^{57}Fe (14.4 keV) we have $\tau_M \cong 1.4 \times 10^{-7}$ s and the emission of the resonance γ-quantum is in this case preceded by K-capture in ^{57}Co with formation of a short-lived ($\tau_0 \cong$ 12.5 ns) 136.4 keV excited state of ^{57}Fe and the subsequent emission of a non-Mössbauer 122 keV γ-quantum (Fig. 4).

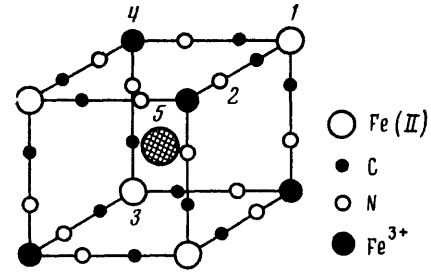


Figure 3. The structures of ferric ferrocyanides: *1*) C atom; *2*) N atom; *3*) low-spin iron atom at a lattice site; *4*) high-spin iron atom at a lattice site; *5*) high-spin iron atom in an interstitial position.

Thus the use of delayed ν (122 keV) and γ (14.4 keV) coincidences with a variable delay time (DMES) leads to the possibility of investigating relaxations with characteristic times ranging from $\tau_r \sim \tau_{coinc} \sim 10^{-9}$ s to $\tau_r \gtrsim \tau_M \cong 10^{-7}$ s.

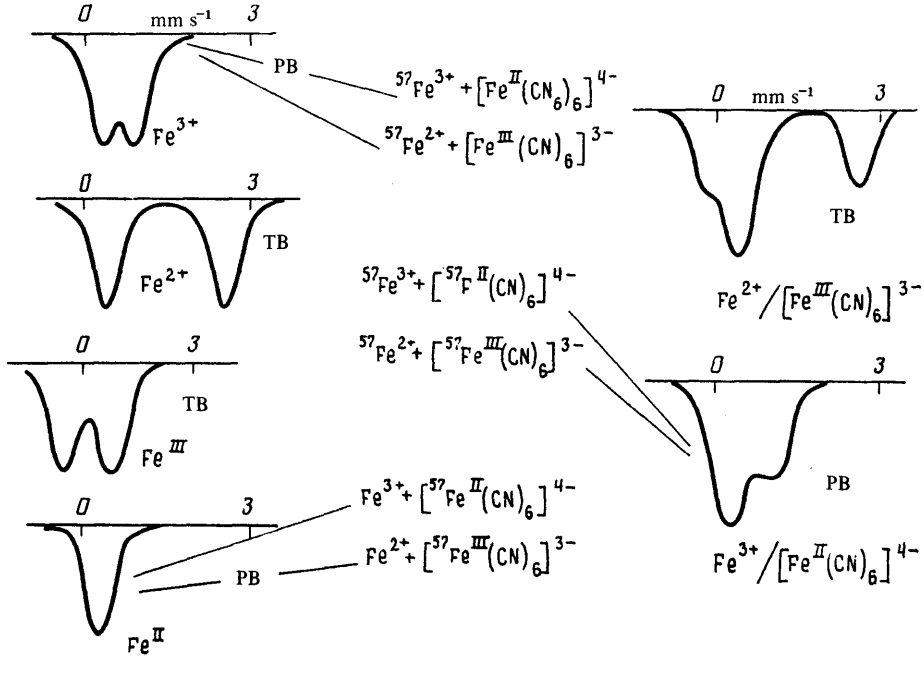


Figure 2. Mössbauer spectra of four different forms of iron.

Various chemical consequences of nuclear transformations, for example, the "shake-up" of the electronic shells as a result of the rapid change of nuclear charge and the subsequent Auger transitions, the Coulombic explosions of multiply ionised molecules, local heating, autoradiolysis, etc., are well known. Here we shall not discuss such processes (they are usually completed before the population of the 14.4 keV level of ^{57}Fe) and shall confine ourselves to chemical relaxation proper. This means, that we shall deal only with systems where the pre-Mössbauer nuclear transformation $^{57}Co \rightarrow {}^{57}Fe$ does not alone lead to an alteration of the ligand environment or the charge state of the daughter Mössbauer atoms (^{57}Fe), which are stabilised in the same environment and in the same valence state as the parent (^{57}Co) radioactive atoms. Since, however, certain chemical (valence and spin) states, which are entirely stable for the parent atom, prove to be unstable for the daughter atom (with an excited Mössbauer nucleus), the system will tend to a stable state, i.e. will undergo chemical relaxation.

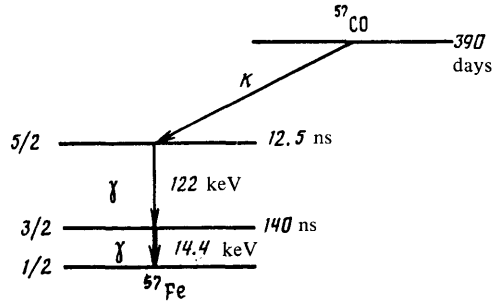


Figure 4. Schematic illustration of the radioactive decomposition (*K* capture) of ^{57}Co and subsequent γ-transitions for ^{57}Fe.

Precisely this situation has been observed[12–16] for ^{57}Co-labelled TB-like compounds of the kind of ferrous cobalticyanide $Fe^{2+}/[^{57}Co^{III}(CN)_6]$ and cobaltous ferricyanide $^{57}Co^{2+}/[Fe^{3+}(CN)_6]$. The decomposition of ^{57}Co is in this case followed by a kind of intramolecular oxidation-reduction reaction, in which the low-spin tervalent iron plays the role of the oxidant and the high-spin bivalent iron acts as the reductant. As a result, TB is rapidly converted into PB and is not therefore manifested in the usual absorption spectra, but it ultimately proved possible to demonstrate the initial formation of the short-lived TB with the aid of MES.

The search for the short-lived TB by MES methods was carried out using both the IMES and DMES (t = 0–60 ns) versions. The experiments with labelled cobalticyanide sources $M^{n+}/[^{57}Co^{III}(CN)_6]^{3-}$, where $M^{n+} = Ni^{2+}$, Co^{2+}, Cu^{2+}, and Fe^{3+} and with the $^{57}Co^{2+}/[Fe^{II}(CN)_6]$ source revealed the formation of daughter ^{57}Fe atoms in the same states as those in which the parent ^{57}Co atoms existed[17,18] and thus demonstrated the absence of appreciable chemical consequences in the emission spectra due to the effect of the *K*-capture in ^{57}Co. The cobaltous ferricyanide $^{57}Co^{2+}/[Fe^{III}.(CN)_6]^{3-}$ was used as the source, while potassium ferrocyanide $K_4Fe^{II}(CN)_6.3H_2O$ served as the absorber in the first MES experiments carried out at 77 K.[12] The results for the IMES and DMES (t = 0–60 ns) versions are presented in Fig. 5.

Subsequent measurements[13] using the IMES version were performed on another source—of the type of cobaltous ferricyanide $Na^{57}Co/Fe^{III}(CN)_6$, and at lower temperatures, down to 12 K (Fig. 6). It is evident that the contribution of the broad Fe^{2+} doublet (which is altogether absent from the absorption spectra owing to the instability of the TB) is in this case much greater than for IMES at 77 K. This fact reflects the retardation of the transformation TB → PB when the temperature is reduced from 77 to 12 K.

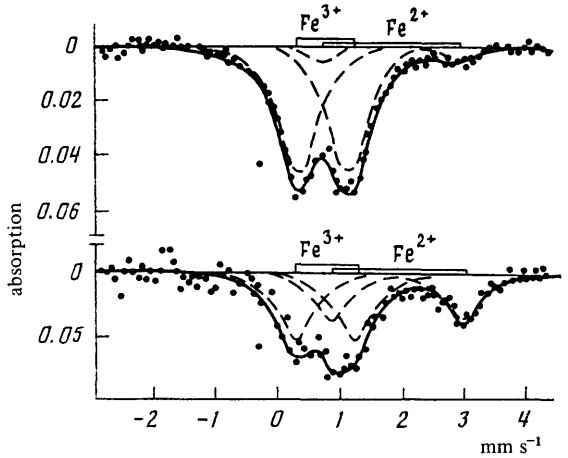


Figure 5. Mössbauer emission spectra of cobaltous ferricyanides $^{57}Co^{2+}/[Fe^{III}(CN)_6]$ at 77 K:[12] above—IMES; below—DMES (0–60 ns). The positions of the peaks of the narrow Fe^{3+} doublet and the broad Fe^{2+} doublet are indicated.

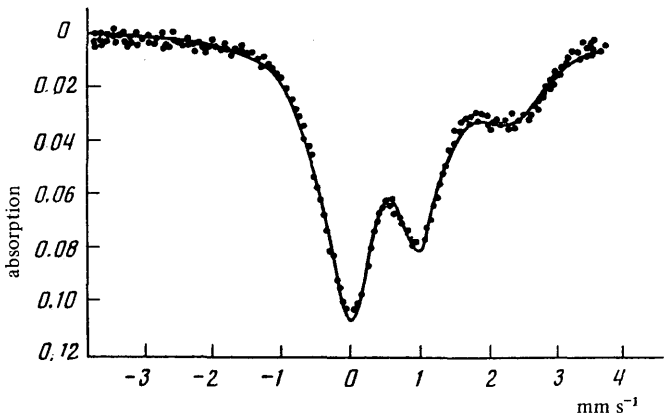


Figure 6. Mössbauer emission spectrum, integrated with respect to time (IMES), of $Na^{57}Co/[Fe^{III}(CN)_6]$ at 12 K.[13]

For an approximate (but sufficiently reliable) estimate of the rate of electron transfer in the transformation TB → PB, we shall employ a simplified representation of the observed emission spectra as a superposition of two undistorted components—the narrow Fe^{3+} (PB) and the broad Fe^{3+} (TB) symmetrical quadrupolar doublets (assuming that in this case

$f_{PB} = f_{TB}$). Under these conditions, the contribution of TB to the DMES spectra, obtained with a "window" of delayed $\gamma\gamma$-coincidences between $t = 0$ and $t = \tau$, should be given by

$$P_\tau = P_0\lambda\,[1 - e^{-(\lambda+k)\tau}]/(\lambda + k)(1 - e^{-\lambda\tau}),$$

where $\lambda = \tau_M^{-1}$, k the rate constant for the chemical transition (TB → PB), and P_0 the initial population of the TB state. With increase of τ, P_τ should diminish, approaching at $\tau \to \infty$ the value $P_\infty = P_0\lambda/(\lambda + k)$, characteristic of measurements by the IMES method.

The values of k obtained in this way in the range from 77 to 400 K are presented on the left-hand side of the curve in Fig. 7.[14] The right-hand side of the curve demonstrates the data obtained over the range 77–12 K with the aid of the IMES version in our joint study with the Helsinki group,[13] using the $Na^{57}Co/[Fe^{III}(CN)_6]$ source. It follows from Fig. 7 that the temperature variation of the rate of electron transfer from Fe^{2+} to $[Fe^{III}(CN)_6]$ gradually changes in accordance with a function of the Arrhenius type at temperatures above approximately 200 K (the activation energy E reaches here the value $E \cong 0.025$ eV) up to the low-temperature plateau at $T \lesssim 50$ K.

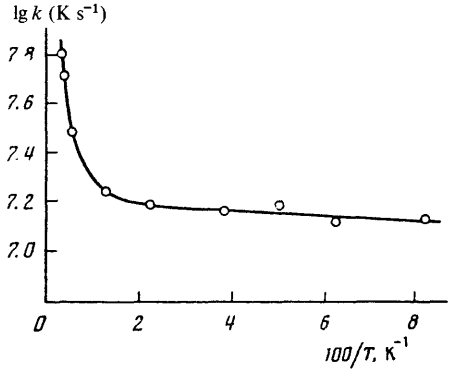


Figure 7. Temperature dependence of the rate constants for the TB → PB transition (data from Refs. 12 and 13 generalised and analysed in Ref. 14).

In this case the study of the rapid intramolecular transfer by the MES method came into contact with another field of our research—the problem of quantum (tunnel) chemical reactivity at low temperatures.

In our early theoretical studies on this problem,[19,20] the criterion of the "tunnel temperature" was introduced:

$$T_t = \frac{\hbar\sqrt{2}}{k_B\pi d}\left(\frac{E}{m}\right)^{1/2}$$

where E is the height and d the width of the activation barrier and m is the mass of the tunnelling species. The high-temperature Arrhenius region is located above T_t, while below T_t is the region of the exponential predominance of tunnelling, which ultimately ensures the attainment of a plateau—the low-temperature quantum limit of the rate of the chemical reaction.

Within the framework of the theory of non-radiative transitions, two types of tunnelling, characteristic of different chemical reactions,[5] are considered and are usually referred to as the electronic-nuclear tunnelling and molecular tunnelling. Both these types of tunnelling lead to the appearance of a low-temperature plateau in the rate of reaction and the presence of such a plateau is regarded as proof that tunnelling predominates. The electronic-nuclear tunnelling was discovered in 1966 by Chance and de Vault in relation to the oxidation of cytochrome *c* by chlorophyll[21] and has also been observed, starting in 1971,[22] for many instances of the long-range electron transfer (over tens of angstroms) between donors and acceptors—variable valence ions.

Molecular tunnelling, observed in the form of a low-temperature plateau in the rate of the "true" chemical reaction in the full sense of these words (which rules out molecular rearrangement, steric rearrangement of atoms, and changes in valence bond lengths and angles) was discovered in 1973 in relation to the polymerisation of formaldehyde.[23]

The conversion of TB into PB was the first observed instance of intramolecular electron transfer via electronic-nuclear tunnelling. In contrast to the tunnelling of free electrons in solid-state physics, their "chemical" tunnelling is associated with the displacement of the nuclei and hence electronic-nuclear tunnelling is associated with a definite breakdown of the Franck–Condon principle.

The probability of a non-radiative electron transfer W_{if} is determined by the overlap of the electronic (ψ_e) and nuclear vibrational (ψ_ν) wave functions in the initial (i) and final (f) states, described respectively by the electron transfer matrix element $L_e^2 = |\langle\psi_{e_i}|\hat{L}|\psi_{e_f}\rangle|^2$ and the Franck–Condon factor $F_\nu = |\langle\psi_{\nu_i}|\psi_{\nu_f}\rangle|^2$:

$$W_{if} = \frac{2\pi}{\hbar} L_e^2 F_\nu \rho_f,$$

where $\hat{L}$ is the transition operator of the type for non-abiabatic conditions and $\rho_f \sim (\hbar\omega)^{-1}$ the density of the vibrational levels in the final state (it is assumed that the dissipation of the heat of exothermic transitions in solids in the form of phonons occurs very rapidly and does not limit the observed rate of reaction).

The electronic-nuclear tunnelling is illustrated schematically on the left-hand side of Fig. 8. The penetration of the electron through the potential barrier (with a width l and a height E) is in this case accompanied by a much smaller barrier-free displacement (d) of nuclei. However, with increase of d whereupon the nuclear shift greatly exceeds the amplitude of the nuclear vibration Δ [for the nth vibration level of a harmonic oscillator, $\Delta_n = (2n + 1)^{1/2}(\hbar/M\omega)^{1/2}$, where M is the nuclear mass and ω the characteristic vibration frequency], a potential barrier to nuclear transfer also appears (Fig. 8*a*) and the possibility of chemical reaction via molecular tunnelling arises. The wave functions $\psi_e(x)$ are proportional to $\exp(-x/\alpha)$ (for $x > \alpha$), where $\alpha = \hbar/(2mE_e)^{1/2}$, and for $l \gg \alpha$ the matrix element L_e^2 assumes the form of a tunnel factor of the Gamow type: $L_e^2 \sim \exp[-\beta l(m_e E_e)^{1/2}/\hbar]$, where $\beta \sim 1$ (and depends on the form of the barrier) and m_e is the mass of the electron.

This expression for L_e^2 is valid in the region of the low-temperature plateau, while above the "tunnelling temperature"

$$T_{te} = \frac{\hbar\sqrt{2}}{k_B\pi l}\left(\frac{E_e}{m_e}\right)^{1/2} \cong 12\,000\,\frac{E_e^{1/2}}{l}$$

(Here E is expressed in eV, l in Å, and T_{te} in K) a temperature dependence of the Arrhenius type is valid:

$$L_e^2 \sim \exp(-E_e/k_B T).$$

The wave functions $\psi_\nu(x)$ are proportional to $\exp[-(x/\Delta)^2]$ (for $x > \Delta$) and, for the Franck–Condon factor can therefore be represented by $F_\nu \sim [\exp-(\kappa d/\Delta)^2]$, where $\kappa \sim 1$. Since the statistically averaged vibration amplitude increases with temperature and for a harmonic oscillator $\langle\Delta^2\rangle$ is proportional to T for $k_B T \gg \hbar\omega$, the behaviour of the Franck–Condon factors at high temperatures is of the Arrhenius type for both barrier-free and sub-barrier nuclear shifts.

With decrease in temperature, whereupon Δ approaches the amplitude of zero-point vibrations, Δ_0, the Franck–Condon factor reaches a minimal constant value (like also L_e^2), which leads to the appearance of a low-temperature plateau in the overall rate (W_{if}) of the non-radiative transition.

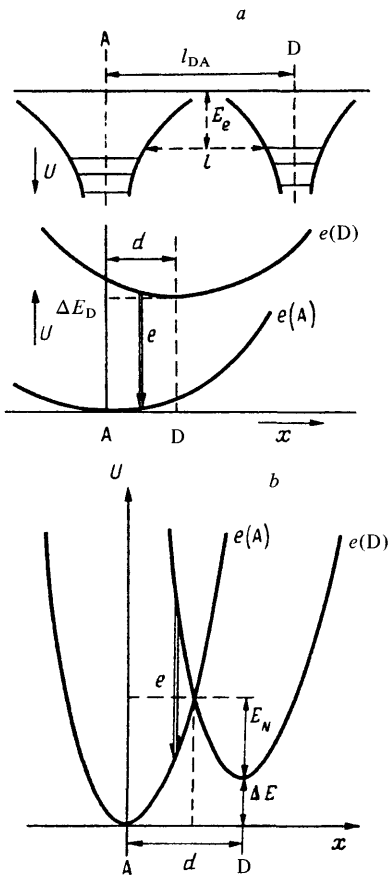


Figure 8. Schematic illustration of the electronic-nuclear tunnelling in electron transfer from a donor (D) to an acceptor (A): *a*) electron tunnelling over a distance l_{DA} through a barrier with a height E_e; such an electron transfer, symbolised below by a vertical arrow between two potential curves for internuclear interaction, corresponding to the states *e*(D) and *e*(A), is accompanied by a barrier-free shift of nuclei over a distance *d*; *b*) the nuclear shift *d* in the electron transfer from the donor to the acceptor is so great that the potential barrier with a height E_N and a width *d* arises between the two *e*(D) and *e*(A) potential curves (the heat of the transition is ΔE).

In the simplest case of resonance nuclear tunnelling, the Franck–Condon factor assumes the Gamow form (see, for example, Jortner and Ulstrup[24]) and the "tunnelling temperature" T_{tN} for the nuclear shift is

$$T_{tN} = \frac{\hbar}{k_B \pi \sqrt{2}\, d}\left(\frac{E_N}{M}\right)^{1/4} \cong 20\,\frac{E_N^{1/4}}{d}$$

(here *E* is expressed in eV, *d* in Å, and T_{tN} in K) for iron nuclei.

The structure of ferric ferrocyanide crystals is well known and corresponds to the interionic electron tunnelling distance $l \sim 5$ Å. The typical energy of charge transfer from the metal to the ligand in complexes of transition metals in the first row is $E_e \cong 4$ eV.[25] Consequently, the tunnelling factor of the Gamow type for a parabolic barrier ($\beta = \pi\sqrt{2}/2$) is close to 2.5×10^{-4}. The overall factor associated with the retardation of the transformation TB → PB on the low-temperature plateau, where the rate constant $k \sim 10^{-7}$ s^{-1}, amounts to $\sim 10^{-7}$, which means that the contribution of the nuclear shift (the Franck–Condon factor) to such retardation is virtually the same as for the tunnelling of the electron:

$$F_v \sim \exp[-(\varkappa d/\Delta_0)^2] \cong 4 \cdot 10^{-4}.$$

The estimated value $\varkappa d/\Delta_0 \sim 2.8$ can be compared with the probability of the Mössbauer effect for PB at low temperatures: $f' = \exp[-(\Delta_0/\lambda)^2] \cong 0.6$, where $\lambda = 0.14$ Å.

Thus $\Delta_0 \cong 0.1$ Å and $\varkappa d \cong 0.3$ Å. Together with $E_A \cong 0.025$ eV, this reasonable estimate corresponds, in the case of a resonance nuclear shift, to $T_t \sim (10\varkappa)$ K and thus confirms the conclusion that it is in fact the nuclear shift and not the electron transfer which is the process determining the appearance of the plateau in the rate of the transformation TB → PB, but only at $T \lesssim 50$ K and not at higher temperatures, where thermally activated electron tunnelling takes place.

Thus the combination of the experimental data for the rate of the chemical reaction on the low-temperature plateau ($\tau_r \cong \tau_M$), of the values of f' at $T \to 0$, and of the tunnelling temperature leads to fairly reliable estimates of both $\varkappa$ and *d*.

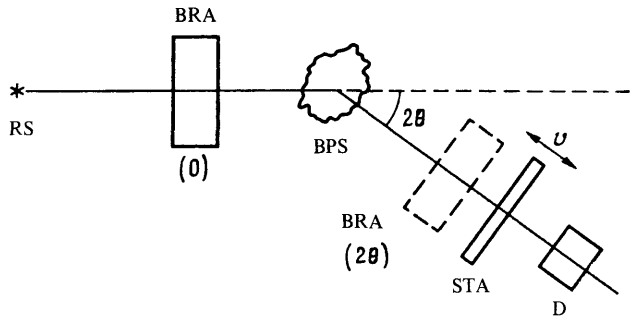


Figure 9. Schematic illustration of experimental observation of the RSME: RS—resonance source; BRA—"black" resonance absorber ensuring effective absorption throughout virtually the entire width of the Mössbauer line (it is placed either before the scatterer or beyond it—at an angle 2θ); BPS—biopolymeric scatterer; STA—standard thin absorber for the measurement of the line form by varying the rate of its movement ν; D—scintillation detector of γ-quanta, operating as the resonance detector together with the BRA.

III. STUDIES OF THE DYNAMIC PROPERTIES OF BIOPOLYMERS BY THE RSME METHOD

Extensive possibilities for the dynamic investigation of various chemical and especially biological systems have arisen as a result of another modern Mössbauer spectroscopic

method—the observation of the Rayleigh scattering of the Mössbauer emission (RSME).[26-38] Leaving to one side its most informative (but also the most difficult to apply) version—coherent RSME, we shall consider only non-coherent scattering data.

The usual Mössbauer method involves the employment of a resonance source and a resonance absorber (or scatterer), while the detector is usually of the non-resonance type. The RSME method is based on the combination of the resonance source and the resonance detector for γ-rays (Fig. 9). The exceptionally high energy resolution of the method ($\sim 10^{-9}$ eV) ensures the possibility of eliminating all non-elastic processes and a reliable determination of the contribution of elastic scattering against their background, where the elastic scattering itself is atomic and not nuclear in nature and takes place on the electron shells. In RSME observations there is therefore no need to have Mössbauer nuclei in the test specimens; Rayleigh scattering can be observed successfully and can yield valuable information for any substances in both solid and liquid phases, in the crystalline and amorphous states, and over wide ranges of temperatures, degrees of hydration, and other variables.

These features in fact determine the advantages of RSME in the study of biopolymers compared with other dynamic methods, the interpretation of the results of which also involves the use of Van Hove correlation functions, such as X-ray dynamic analysis (XDA) [39-41] and the usual MAS.[42-45]

Table 2. Biopolymers investigated by the method based on the Rayleigh scattering of the Mössbauer emission (RSME) and the information obtained.

Substance	MW	Information*	Refs.
Metmyoglobin (of the whale)	17 800	$f_R(T)$, $\Delta\Gamma_R(T)$ (T=100—300 K; h=0,05—2.3; (crystal)	[33. 46]
Trypsin	23 300	$f_R(T)$; $\Delta\Gamma_R(T)$ (T=100—300 K; h=0.1; 0.5; 0,8); $f_R(h)$ at $T \approx 300$ K (h=0.1—1)	[36]
Human serum albumin (HSA)	66 500	$f_R(T)$; $\Delta\Gamma_R(T)$; $f_R(h)$ (T = =100—300 K; h=0.1—0.7); $f_R(\eta)$	[37. 38]
Chromatophores:			
Rhodospirillum Rubrum	$\sim 10^7$	$f_R(T)$; $f_R(h)$	[34]
Ect. Shaposhnikovii	$\sim 10^7$	$f_R(T)$; $f_R(h)$; $f_R(\eta)$	[35]
DNA (from ox spleen)	$(1.5-3.0)\cdot 10^6$	$f_R(T)$; $\Delta\Gamma_R(T)$; $f_R(h)$	[46]

*The information obtained represents the functional dependence of the probability of the elastic RSME (f_R) and of the width of the RSME resonance line (Γ_R) on the temperature T, the degree of hydration h (grammes of water per gramme of biopolymer), and the viscosity of the surrounding medium η. The viscosity was varied by adding glycerol (HSA, chromatophores) and glutaraldehyde (HSA).

A general description of the RSME theory and methods is available in a number of communications (see, for example, Refs. 26—28), while our previous studies (for example, Refs. 29—38) were concerned with both theoretical and experimental aspects of the application of incoherent RSME to the study of the dynamic properties of biopolymers. Here we shall confine ourselves to the description of certain typical results and the most important conclusions. The biopolymers investigated and the conditions in their study (temperature, degree of hydration) are listed in Table 2.

The probability f_R of the elastic RSME served as the fundamental initial dynamic characteristic of all the objects studied. This probability is proportional to the generalised Debye—Waller factor:

$$\exp(-2W) = \exp(-Q^2\langle x^2\rangle)$$

(here $Q = 4\pi \sin\theta/\lambda$ is the momentum transferred in scattering through an angle 2θ) and thus makes it possible to determine the averaged, generalised mean-square shift $\langle x^2\rangle$, which is assumed to be the same, in such general treatment, for all the atoms of the test specimens.

Additional dynamic information can be obtained by analysing the shape of the RSME spectral lines and by comparing the observed changes in this shape (or its constancy) with the expected increase of the line width Γ_R with decrease of f_R.[29-38]

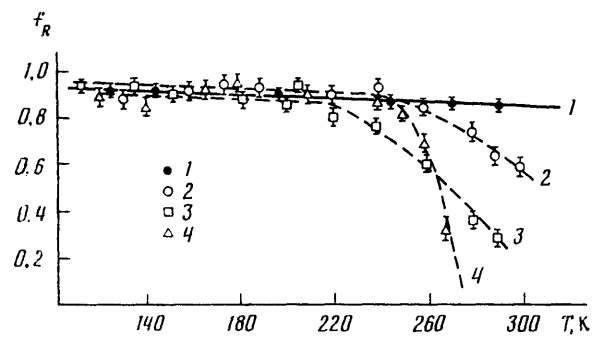


Figure 10. The contribution of elastic scattering as a function of temperature for different metmyoglobin specimens:[33] *1*) for $P/P_S = 0.37$ ($h = 0.05$); *2*) crystalline metmyoglobin; *3*) for $P/P_S = 0.94$ ($h = 0.5$); *4*) aqueous solution (26.6% metmyoglobin; $h = 2.3$).

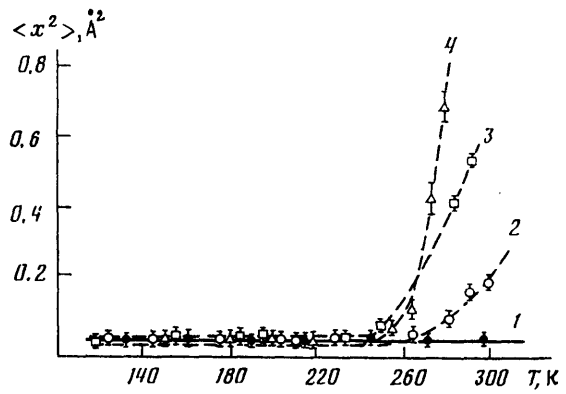


Figure 11. Generalised mean-square shift $\langle x^2\rangle$ as a function of temperature for different metmyoglobin specimens;[33] for the designation of the curves and points, see the legend to Fig. 10.

A characteristic feature of the spectra of all the hydrated specimens (with a degree of hydration $h \gtrsim 0.3$ g of water per gramme of the biopolymer) was a sharp decrease of f_R at $T \gtrsim 220$–230 K, i.e. a sharp increase of the generalised mean-square shift, which reached extremely high values: $\langle x^2 \rangle \cong 1$ Å^2 for $h \cong 0.7$ and $T \cong 300$ K,[37] while the decrease of f_R at $T = 100$–300 K for dry specimens ($h \cong 0.05$) is linear and altogether insignificant: for example, $\langle x^2 \rangle \cong 0.05$ Å^2 at $T \cong 300$ K.[35]

The temperature variations of f_R and $\langle x^2 \rangle$ for metmyoglobin for different values of h [31] are presented in Figs.10 and 11. These data reveal a characteristic feature of the dynamics of biopolymers—a sharp decrease of f_r and a corresponding increase of $\langle x^2 \rangle$ in the high-temperature ($T \gtrsim 220$ K) region with increase of the degree of hydration h.

A typical example is provided by human serum albumin (HSA) at $T \cong 300$ K (Fig.12). The observed dependence of f_R on h is in this case much more pronounced than might have been expected if the mobilities of the protein as such and of the much more mobile solvent (water) had been additive. Even for high degrees of hydration ($h \cong 0.8$), the added portions of water continue to cause additional loosening of the proteins increasing the mobility of the protein globule.

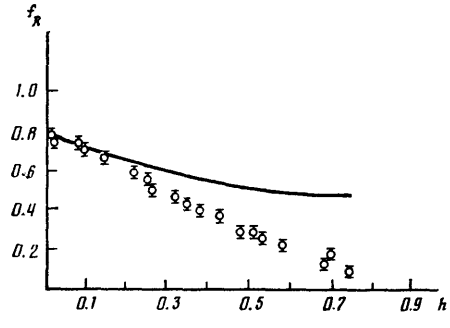


Figure 12. The contribution of elastic RSME as a function of the degree of hydration for human serum albumin at 300 K: symbols—experimental data; curve—calculation assuming simple additivity (without any correlations between the values of f_R for the protein and the solvent).[38]

The dependence of the generalised Debye–Waller factor for biopolymers on two parameters—temperature and degree of hydration—can be represented by a three-dimensional f_R (T, h) diagram, illustrated schematically in Fig.13.

The sharp decrease of the probability of the elastic RSME for biopolymers with increase of D and h is not accompanied by any serious broadening ($\Delta\Gamma$) of the spectral line. For example, the shapes of the RSME $g(\omega)$ lines for crystalline metmyoglobin at 240 and 300 K are virtually identical (Fig.14), while an almost fourfold decrease of f_R for HSA with increase of the degree of hydration (from $h = 0.05$ to $h = 0.73$) is accompanied by only a slight ($\Delta\Gamma \cong 0.10$ mm s^{-1}) broadening of the principal, "narrow" component of the RSME spectrum and by the appearance of a fairly weak broad component (Fig.15).

Such properties of the RSME spectra of biopolymers can be described by neither the Debye nor the Einstein models of the solid state nor by the picture representing a free liquid with spatially unlimited diffusion, to which the relation $f_R \cong \Gamma/(\Gamma + \Delta\Gamma)$ would have corresponded. Since the temperature dependence of the Debye–Waller factors and the line width for RSME is very similar to that for MAS (however, hydration effects have not been investigated by the MAS method), the RSME data can be interpreted by the procedures developed in recent years for the analysis of MAS results (see, for example, Refs.47–51) and based on the model representing continuous spatially limited diffusion, i.e. a Brownian harmonic oscillator with pronounced decay.

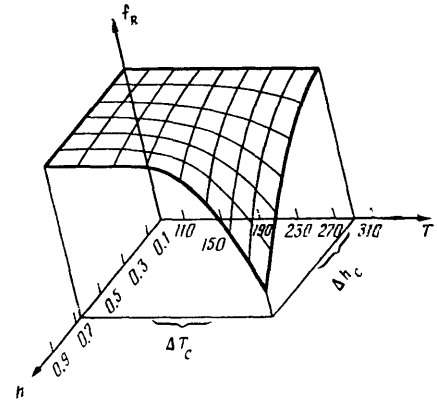


Figure 13. Three-dimensional diagram illustrating the dependence of the contribution by the elastic RSME on temperature and the degree of hydration.[46]

The physical foundations for such an approach appeared in 1973–1979 in the form of the idea of the existence of conformational substates (CSS) or, in other words, quasi-degenerate conformational states (QDCS) of protein globules, i.e. surfaces of a given macromolecule with the same overall structure which are almost degenerate in terms of energy and differ only slightly in terms of the local configurations.

Regardless of the approach to the treatment of QDCS [as "mobile defects",[52] treatment aided by the computer modelling of the dynamic properties of proteins[53] on the basis of the polychromatic kinetics of the Fe–CO recombination in haem-containing proteins,[54,55] or X-ray-dynamic analysis (XDA) [39–41]], the QDCS concept implies a definite modification of the understanding of protein structure (the structure of biopolymers in general) in the spirit of the scheme illustrated in Fig.16. Until the appearance of the QDCS concept, it was usually assumed that, in conformity with the familiar Schrödinger[56] definition of a protein as an aperiodic crystal, each individual biomacromolecule in its ground state is located in a global energy minimum and is characterised by a definite clearly fixed geometry. Within the framework of the QDCS concept, the global energy minimum for biomacromolecules is not realised at all, even as $T \to 0$, and the actual observed state is a spatially delocalised system with numerous local energy minima. The increase of the mobility of biopolymers with increase in temperature and in the degree of hydration can be described by the theoretical methods developed previously[47–51] by virtue of the stimulation of transitions between the QDCS.

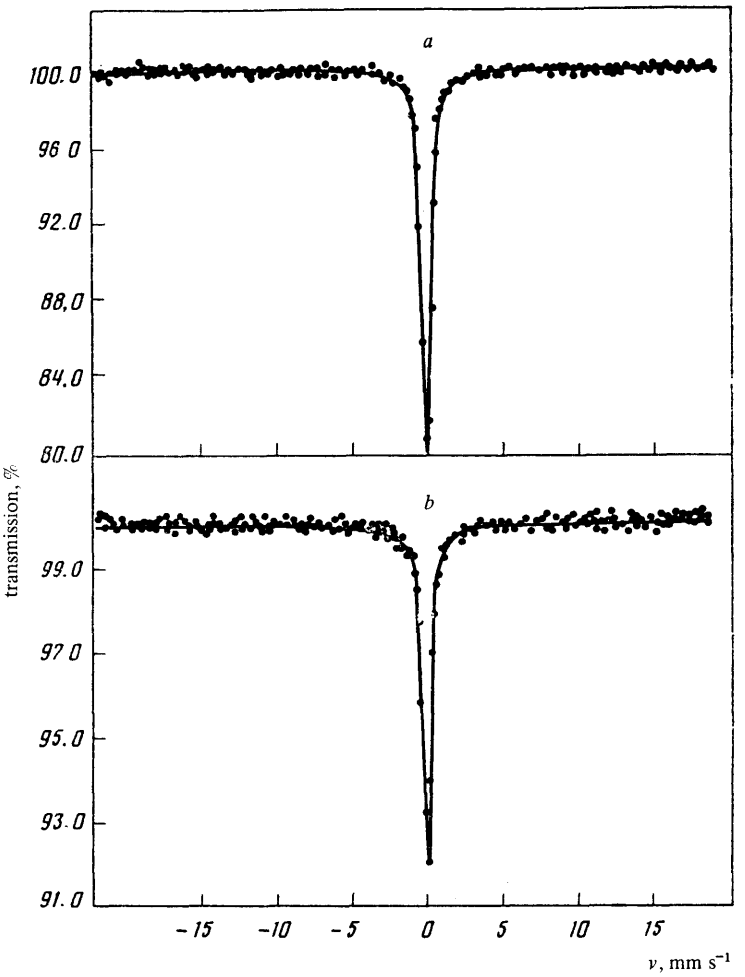


Figure 14. The RSME energy spectra for crystalline metmyoglobin at 240 K (*a*) and 300 K (*b*).[46]

The expansion of the variety of experimental MAS and RSME data necessitates further development of spatially limited diffusion models, namely a transition from the case of a single oscillator to a multimodal approximation, which presupposes the presence of at least two or three Brownian oscillators with pronounced decay. The conformational mobility of biopolymers at room temperature, determined by the MAS and RSME methods, is characterised by a fairly broad spectrum of correlation times τ_c—from 10^{-6} s (broadening of the principal, narrow, spectral line) to 10^{-9} s (contribution to the broad component) and further to even lower values of τ_c (decrease of the contribution of elastic scattering). According to data obtained by other methods (for example, the luminescence and spin label methods[57]), the range of correlation times embraces also much slower movements—down to $\tau_c \sim 1$ s. The hierarchy of the amplitudes and relaxation times of various internal motions in biopolymers is also manifested in the computer modelling of protein dynamics.[58]

A broad spectrum of relaxation times of motions is typical for the vitreous state—in contrast to the liquid and crystalline states.[59] That it is natural to compare the dynamic properties of biopolymers and glasses follows from the entire set of data for the dependence of the RSME spectra on temperature and the degree of hydration. The sharp increase of $\langle x^2 \rangle$ at the glass point T_g, similar to that observed for proteins above $T_c \cong 220$ K and also sometimes accompanied by a slight broadening of the spectral lines (when $f_R \lesssim 0.5$ to 0.1), is typical for supercooled organic liquids.[27,28] Our observations also demonstrated a clear correlation between the onset of the sharp decrease of f_R and the jump in the specific heat following an increase in temperature (DNA: $h \cong 0.6$; $T \cong 200$ K) and in the degree of hydration (lysozyme: $T \cong 300$ K; $h \cong 0.2$–0.3).[33,46] Such jumps in specific heat usually indicate the occurrence of glass points for polymers—they are absent only for a very high ($\gtrsim$75%) degree of crystallinity of the polymers. Additional experimental data, supporting the analogy between the dynamic properties of biopolymers and glasses, are presented and discussed in the present author's more detailed publications.[33,46]

Turning now to the three-dimensional diagram in Fig. 13, it is natural to suppose that, below some kind of "critical" point (more correctly some kind of extended "critical" regions) in temperature and degree of hydration, the ground

state of the biopolymer is more likely to resemble a heterogeneous glass than a crystal. As regards structural characteristics, this approach to biopolymers is consistent with Fig. 16*b*—a system of local energy minima, which implies the absence of structural unambiguity in the biomacromolecule represented by a set of QDCS.

As regards the dynamic characteristics of biopolymers, we employed their heat capacity at very low temperatures as a test of dynamic vitreous properties.[46,64,65] The temperature dependence of the heat capacities of inorganic and organic dielectric glasses at low temperatures is given by

$$C_v(T) = C_1 T + C_3 T^3 + C_E \left(\frac{\theta_E}{T}\right)^2 \cdot \exp\left(\frac{\theta_E}{T}\right) \cdot \left[\exp\left(\frac{\theta_E}{T}\right) - 1\right]^{-2},$$

i.e., apart from the Debye (second) and Einstein (third) terms, it contains a linear term, which predominates as $T \to 0$.[60]

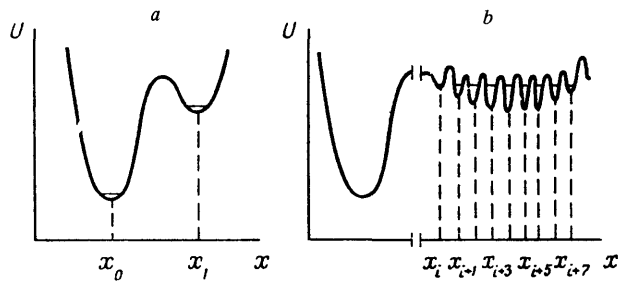


Figure 16. Potential energy curves for biomacromolecules: *a*) global energy minimum corresponds to the ground state (whose structure is unambiguously fixed as $T \to 0$), while the other minima (only one of these is shown) correspond to short-lived and weakly populated excited states; *b*) there is no global minimum at all and the system of local minima represents the spatially delocalised and energetically similar conformational substates (CSS) or quasi-degenerate conformational states (QDCS) whose populations are not unambiguously defined even as $T \to 0$.[46]

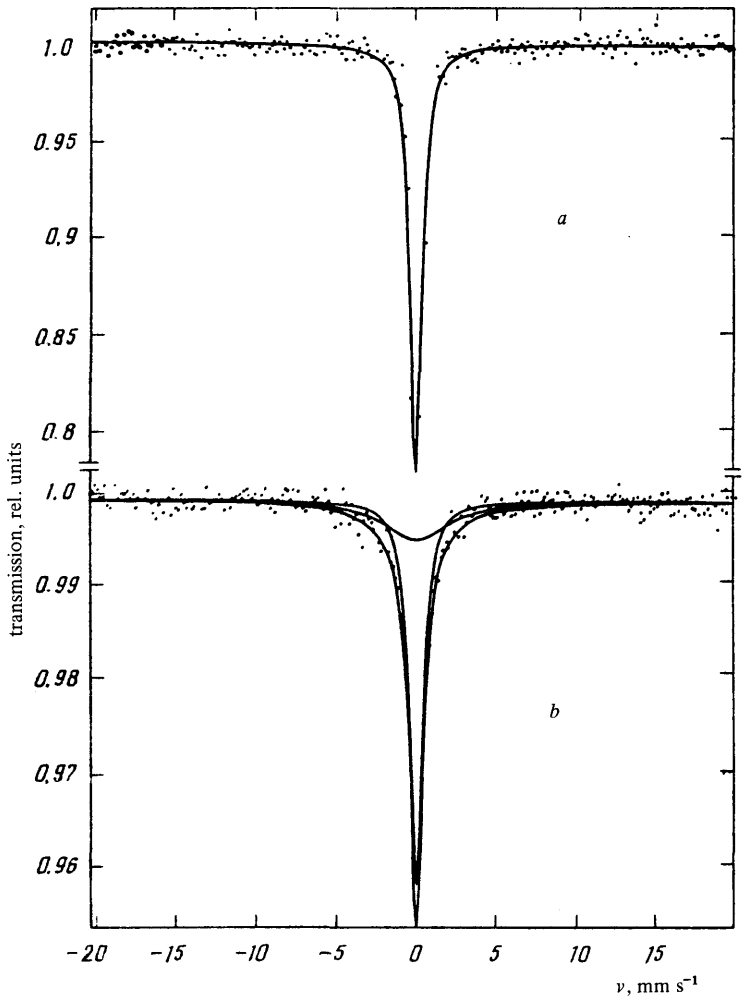


Figure 15. The energy spectra for HSA (300 K) at $h = 0.05$ (*a*) and $h = 0.73$ (*b*). For HAS with $h = 0.73$ (*b*), the overall spectrum represents a superposition of the "narrow" component (with the same line width as for $h = 0.05$) and the "broad" component, which are also illustrated in part *b* of the figure.[37]

This especially important linear contribution to the low-temperature heat capacity is associated with a fundamental property of the vitreous state—its non-equilibrium nature, the existence of a residual entropy as $T \to 0$. Its presence, magnitude, and physical significance have been explained[61,62] on the basis of the model of phonon-stimulated tunnelling (PST) in the so-called two-level (multilevel) systems, i.e. the tunnelling of atoms and atomic groups between two (or many) quasi-equilibrium positions (QEP), between two (or many) similar but non-equivalent potential wells by virtue of the adjustment of the transitional resonance between such QEP via the excitation (absorption or emission) of phonons (Fig.17).

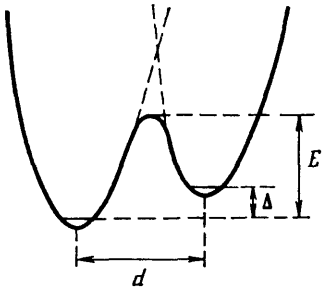


Figure 17. The simplest picture comprising two quasi-equilibrium positions (QEP) for atoms or atomic groups of biopolymer molecules (two-level system with two wells). Typical values: $E \cong 0.2-0.4$ eV, $d \cong 0.2-0.4$ Å. The resonance adjustment within the limits of the width of the energy gap Δ is ensured by phonons (phonon-stimulated tunnelling).[46]

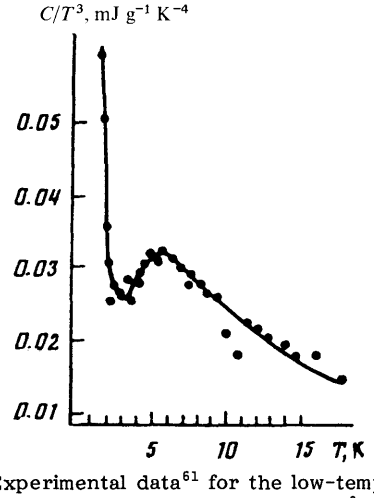


Figure 18. Experimental data[61] for the low-temperature heat capacity of HSA in terms of the function $C/T^3 = f(T)$, illustrating the presence of a linear term due to the phonon-stimulated tunnelling.

The dependence of the quantity C_1 on the spectral density of two-level states $n(\Delta)$ at $\Delta \to 0$ has the following form:[60]

$$C_1 = \frac{\pi^2}{6} k_B^2 n(0).$$

The local energy minima, illustrated in Fig.16*b* and characterising the QDCS of biomacromolecules, form precisely such a multilevel, multiwell system and it is natural to expect the occurrence of PST between QDCS playing the role of QEP.

We have analysed extensive experimental data for the low-temperature heat capacities of biopolymers (see the relevant review[63]) on the basis of the above three-term formula and observed[33,64,65] that the linear term C_1T for biomacromolecules is significant.

The results of our calculations and also of later direct experiments with HSA [66] (Fig.18) and metmyoglobin [67] are compiled in Table 3.

Table 3. Parameters of the low-temperature heat capacities of polymers and biopolymers.

Substance	C_1, $\mu J\ g^{-1}\ K^{-2}$	C_3, $\mu J\ g^{-1}\ K^{-4}$	$10^{-40} n(0)$, $J^{-1}\ g^{-1}$	Number of two-well systems (for $\Delta = 100$ K)	Temperature range of measurements ΔT, K	Refs.
SiO_2	1.2	1.8	0.38	—	0.1—1 5	[60]
Poly(methyl methacrylate)	4 8	28	1.5	—	1,5—10	[60]
Melanine (1% H_2O)	5.0	12	1.6	—	2—4 5	[68]
Melanine (20% DCA)	9.5	9.9	3	—	2—4.5	[68]
Melanosoma	22	9.9	7	—	2—4.5	[68]
Poly-L-alanine (α-form)	45	25	14	—	1.5—10	[69]
Poly-L-alanine (β-form)	36	20	11	—	1.5—10	[69]
Polyglycine-P	18	8.8	59	—	1 5—22	[70]
Collagen	$\sim 10^3$	10	300	$2.5 \cdot 10^3$	5—20	[63]
DNA	~ 10		3.2	$2.1 \cdot 10^3$	0.5—5	[71]
HSA	39	8	12.5	19	1.5—25	[66]
Metmyoglobin	—	—	3.3	1.4	0.1—3	[67]

The vitreous dynamic model of biopolymers proposed by the present author and his co-workers[33,64,65] presupposes the existence of internal mobility of the biomacromolecules even as $T \to 0$ by virtue of the PST of atoms and atomic groups.

Thus we have demonstrated yet again that the modern Mössbauer spectroscopic methods constitute an effective instrument in the study of tunnelling phenomena in chemical and biochemical physics—the quantum effects in the kinetics of chemical reactions and biomolecular dynamics, which are most pronounced at low temperatures.

The RSME data can yield fairly reliable estimates of the tunnelling parameters.[33,46] The maximum values of $\langle x^2 \rangle$ at 300 K reach almost 1 Å^2 and the contribution by elastic RSME is in this case smaller by a factor $N = 4-5$ than at low temperatures. According to Shaitan,[72] the factor N means simply the number of potential wells in the multiwell region of the delocalisation of certain atomic groups. The distance between the wells is then given by $d \cong \sqrt{\langle x^2 \rangle}/(N-1) \cong 0.25$ to 0.33 Å; subsequent analysis of the temperature dependence of the parameters of three-dimensional diffusion[47-51] yields the height of the energy barrier between the wells: $E \cong 0.2$ eV and the tunnelling temperature[19,20] for CH_2 groups is accordingly estimated at $T_t \cong 120-160$ K. Inspection of the multimodal Franck–Condon effects, i.e. allowance for the low-frequency vibrations of potential wells relative to one another[73-75] (apart from the high-frequency vibrations of the tunnelling groups within the limits of the occupied wells) leads to the conclusion that, even at the physiological temperatures, the contribution of tunnelling may be quite comparable to that of thermally activated transitions of atomic groups between QEP and that tunnelling induced by fluctuations can have a definite importance also for the functioning of proteins and other biopolymers.[33,46]

Thus RSME studies on biopolymers combined with MAS and XDA data as well as low-temperature heat capacities provide an adequate basis for treating natural biopolymers as special heterogeneous glasses incorporating regions with different glass points.[33,46,64,65]

At room temperature, a biomacromolecule contains regions whose properties resemble those of a crystal, a glass, a supercooled liquid, and an ordinary liquid. The principal physical parameter, chosen here for the purpose of the description and comparison of different states, is the free volume.

The $f_R(T, h)$ three dimensional diagram (Fig.13) demonstrates the existence of a transitional ΔT_c region in the vicinity of $T_c \cong 200-220$ K and a Δh_c region in the vicinity of $h_c \cong 0.1-0.3$. For $T < T_c$ and $h < h_c$, the dynamic properties of biopolymers combine the properties of a crystal and a glass, while above T_c and h_c they combine the properties of a crystal, a glass, and a supercooled liquid.

The temperature T_c plays the role of the usual glass point T_g and the degree of hydration h_c plays the role of a kind of hydration glass point h_g for those regions in biomacromolecules where the glass state is transformed into the highly elastic state. The increase of the specific volume (and also of the free volume) of the biopolymer and hence of its internal mobility with increase of temperature and of the degree of hydration accelerates appreciably at temperatures above T_c and for $h > h_c$.

All the above considerations are summarised in Table 4, where the plus and minus signs denote the presence or absence of the following four main properties: (a) order; (b) periodicity of the structure (for an individual biomacromolecule); (c) unambiguity of the structure (for an individual biomacromolecule) as $T \to 0$; here the plus sign denotes that $S_0 = 0$ at $T = 0$ and the minus sign denotes that $S_0 \neq 0$; (d) mobility as $T \to 0$.

Table 4. Description of the parameters of the structural and dynamic properties of biopolymers.

Substance	Order	Periodicity	Unambiguity of structure*	Mobility*	Glass:IC number***
Ideal crystal	+	+	+	−	
Glass	−	−	−	+**	
Aperiodic crystal	+	−	+	−	1:3
Biopolymer (treatment after 1973-1979)	+	−	−	−	2:2
Biopolymer (treatment after 1983)	+	−	−	+	3:1

*As $T \to 0$.
**Treatment after 1972.
***Here IC = ideal crystal.

The ideal crystal (+++−) and glass (−−−+) (the plus sign denoting mobility in glasses has been generally accepted since 1972 [61,62]) are used in Table 4 as the principal comparison standards. The Schrödinger definition[46] of the protein as an aperiodic crystal is designated by the symbol (+−+−), the appearance of the concept of CSS (QDCS) (1973–1979) [39–41, 52–55] denotes the transition to (+−−−), and finally the vitreous dynamic model of proteins (1983) [33,64,65] corresponds to the formulation (+−−+). Thus the general ratio 3:1 in favour of the ideal crystal has gradually changed to 1:3 in favour of glass.

---o0o---

We have thus seen that gamma-resonance spectroscopy in its MAS and RSME versions has played a very notable role in the development of ideas about the structural and dynamic properties of biopolymers, i.e. in one of the most important problems of modern biochemical physics.

REFERENCES

1. V.I.Gol'danskii, "Effekt Messbauem i Ego Primenenie v Khimii" (The Mössbauer Effect and Its Chemical Applications), Izd.Akad.Nauk SSSR, Moscow, 1963.
2. V.I.Gol'danskii and R.H.Herber (Editors), "Chemical Applications of Mössbauer Spectroscopy", Acad.Press, New York, 1968.
3. V.I.Gol'danskii, "Fizicheskaya Khimiya Pozitrona i Pozitroniya" (Physical Chemistry of the Positron and Positronium), Izd.Nauka, Moscow, 1968.
4. V.I.Goldanskii, Acc.Chem.Res., 1977, **10**, 153.
5. V.I.Goldanskii, Nature, 1979, **279**, 109.
6. R.P.Bell, "The Tunnel Effect in Chemistry", Chapman and Hall, London, 1980.
7. V.I.Gol'danskii, L.I.Trakhtenberg, and V.N.Flerov, "Sovremennye Predstavleniya o Tunnelirovanii Tyazhelykh Chastits v Khimicheskikh Prevrashcheniyakh. Itogi Nauki i Tekhniki. Ser.Khimiya Tverdogo Tela" (Modern Ideas about the Tunnelling of Heavy Particles in Chemical Reactions. Advances in Science and Engineering. Chemistry of the Solid State Series), Izd.VINITI, Moscow, 1986, Vol.3.
8. V.I.Gol'danskii, L.I.Trakhtenberg, and V.N.Flerov, "Tunnel'nye Yavleniya i Khimicheskoi Fizike" (Tunnel Phenomena in Chemical Physics), Izd.Nauka, Moscow, 1986.
9. L.A.Blyumenfel'd, V.I.Gol'danskii, M.I.Podgoretskii, and D.S.Chernavskii, Zhur.Strukt.Khim., 1967, **8**, 770.
10. V.I.Goldanskii and R.A.Stukan, J.Radioanal.Chem., 1980, **57**, 299.
11. B.V.Borshchagovskii, V.I.Gol'danskii, G.B.Seifer, and R.A.Stukan, Izv.Akad.Nauk SSSR, Ser.Khim., 1971, 933.
12. V.P.Alekseev, V.I.Gol'danskii, V.E.Prusakov, A.V.Nefed'ev, and R.A.Stukan, Pis'ma v Zhur. Eksper.Teor.Fiz., 1972, **16**, 65.
13. V.I.Gol'danskii, R.A.Stukan, V.E.Prusakov, T.Katila, K.Riski, and Y.Ylä-Jääski, "Abstracts of XX AMPERE Congress", Tallinn, 1978.
14. V.I.Goldanskii and R.A.Stukan, J.de Phys., 1980, **41**, C1–43.
15. V.I.Gol'danskii and R.A.Stukan, Radiokhimiya, 1981, **23**, 473.
16. V.I.Goldanskii, Pure Appl.Chem., 1983, **55**, 11.
17. V.E.Prusakov, R.A.Stukan, B.V.Borshchagovskii, and V.I.Gol'danskii, Teor.Eksper.Khim., 1973, **9**, 707.
18. V.E.Prusakov, R.A.Stukan, B.V.Borshchagovskii, and V.I.Gol'danskii, Radiokhimiya, 1974, **16**, 70.
19. V.I.Gol'danskii, Dokl.Akad.Nauk SSSR, 1959, **124**, 1261.
20. V.I.Gol'danskii, Dokl.Akad.Nauk SSSR, 1959, **127**, 1937.
21. D.De Vault and B.Chance, Biophys.J., 1966, **6**, 825.
22. K.I.Zamaraev, R.F.Khairutdinov, A.I.Mikhailov, and V.I.Gol'danskii, Dokl.Akad.Nauk SSSR, 1971, **199**, 640.

23. V.I.Goldanskii, M.D.Frank-Kamenetskii, and I.M.Barkalov, Science, 1973, **182**, 1344.
24. J.Jortner and J.Ulstrup, Chem.Phys.Letters, 1979, **63**, 236.
25. R.Grimm, P.Gütlich, E.Kankeleit, and R.Limk, J.Chem.Phys., 1977, **67**, 5491.
26. D.A.O'Connor, "Proceedings of the International Conference on Mössbauer Spectroscopy", Cracow, 1975, p.396.
27. D.C.Champeney, Rep.Progr.Phys., 1979, **42**, 1017.
28. G.Albanese and A.Deriu, Riv.Nuovo Cim., 1979, **2**, 9.
29. E.E.Gaubman, Y.F.Krupyanskii, V.I.Gol'danskii, T.V.Zhuravleva, and I.P.Suzdalev, Zhur.Eksper. Teor.Fiz., 1977, **72**, 2172.
30. Yu.F.Krupyanskii, F.Parak, J.Hannon, E.E.Gaubman, V.I.Gol'danskii, I.P.Suzdalev, and K.Hermes, Zhur. Eksper.Teor.Fiz., 1980, **79**, 63.
31. Yu.F.Krupyanskii, F.Parak, V.I.Goldanskii, R.L.Mössbauer, E.E.Gaubmann, H.Engelmann, and I.P.Suzdalev, Z.Naturforsch., 1982, **37C**, 57.
32. V.I. Gol'danskii. Yu.F.Krupyanskii, and E.N.Frolov, Mol.Biol., 1983, **17**, 532.
33. V.I.Goldanskii and Yu.F.Krupyanskii, "Proceedings of the International Congress on Applications of Mössbauer Effect (Alma-Ata, 1983)", Gordon and Breach, New York, Vol.1, p.83.
34. Yu.F.Krupyanskii, K.V.Shaitan, E.E.Gaubman, V.I.Gol'danskii, A.B.Rubin, I.P.Suzdalev, and M.F.Shchukin, Biofizika, 1981, **26**, 1037.
35. Ju.F.Krupyanskii, D.Bade, I.V.Sharkevich, N.Ya.Uspenskaya, A.A.Kononenko, I.P.Suzdalev, F.Parak, V.I.Goldanskii, R.L.Mossbauer, and A.B.Rubin, Europ.Biophys.J., 1985, **12**, 107.
36. Yu.F.Krupyanskii, I.V.Sharkevich, N.V.Medvedeva, Yu.I.Khurgin, I.P.Suzdalev, and V.I.Gol'danskii, Mol.Biol., 1986, **20**, 1356.
37. I.V.Kurinov, Yu.F.Krupyanskii, I.P.Suzdalev, and V.I.Gol'danskii, Dokl.Akad.Nauk SSSR, 1986, **290**, 738.
38. I.V.Kurinov, Yu.F.Krupyanskii, I.P.Suzdalev, and V.I.Goldanskii, Hyperfine Interactions, 1987, **33**, 223.
39. H.Frauenfelder, G.Petsko, and D.Tsernoglou, Nature, 1979, **280**, 558.
40. P.G.Artymiuk, C.C.F.Blake, D.B.P.Grace, S.Y.Calley, D.C.Phillips, and H.J.E.Sternberg, Nature, 1979, **280**, 563.
41. H.Hartmann, F.Parak, W.Steigemann, G.A.Petsko, D.P.Ponsi, and H.Frauenfelder, Proc.Nat.Acad.Sci. USA, 1982, **79**, 4967.
42. H.Keller and P.Debrunner, Phys.Rev.Letters, 1980, **45**, 68.
43. F.Parak, E.N.Frolov, R.L.Mossbauer, and V.I.Goldanskii, J.Mol.Biol., 1981, **145**, 825.
44. F.Parak, E.W.Knapp, and D.Kucheida, J.Mol.Biol., 1982, **161**, 177.
45. E.R.Bauminger, S.G.Cohen, T.Nowik, S.Ofer, and J.Yariv, Proc.Nat.Acad.Sci.USA, 1983, **80**, 736.
46. V.I.Goldanskii, Yu.F.Krupyanskii, and V.N.Fleurov, Phys.Scripta, 1986, **33**, 527.
47. K.V.Shaitan and A.B.Rubin, Biofizika, 1980, **25**, 796.
48. E.W.Knapp, S.F.Fischer, and F.Parak, J.Chem. Phys., 1983, **78**, 4701.
49. K.V.Shaitan and A.B.Rubin, Biofizika, 1984, **29**, 735.
50. F.Parak and E.W.Knapp, Proc.Nat.Acad.Sci.USA, 1984, **81**, 7088.
51. I.Nowik, E.R.Bauminger, S.C.Dohen, and S.Ofer, Phys.Rev.A, 1985, **31**, 2291.
52. R.Lumry and A.Rosenberg, Colloq.Intern.CNRS, 1975, **246**, 53.
53. A.McCammon, B.R.Gelin, and M.Karplus, Nature, 1977, **267**, 585.
54. R.H.Austin, K.Beeson, L.Eisenstein, H.Frauenfelder, I.C.Gunsalus, and V.P.Marshall, Biochemistry, 1973, **181**, 541.
55. R.H.Austin, K.Beeson, L.Eisenstein, and H.Frauenfelder, Phys.Rev.Letters, 1974, **32**, 403.
56. E.Schrödinger, "What is Life from the Standpoint of Physics?" (Translated into Russian), Inostr.Lit., Moscow, 1947.
57. G.I.Likhtenshtein and A.I.Kotel'nikov, Mol.Biol., 1983, **17**, 398.
58. A.McCammon and M.Carplus, Acc.Chem.Res., 1983, **16**, 187.
59. V.N.Fleurov, Sov.Phys.-Solid State, 1984, **35**, 134.
60. "Amorphous Solids. Low Temperature Properties. Topics in Current Physics", Springer, Berlin, 1981, Vol.24.
61. P.W.Anderson, B.J.Halperin, and C.M.Varma, Phil. Mag., 1972, **25**, 1.
62. W.A.Phillips, Low Temp.Phys., 1972, **7**, 351.
63. G.N.Mrevlishvili, Uspekhi Fiz.Nauk, 1979, **27**, 273.
64. V.I.Gol'danskii, Yu.F.Krupyanskii, and V.N.Flerov, Dokl.Akad.Nauk SSSR, 1983, **272**, 978.
65. V.I.Gol'danskii and Yu.F.Krupyanskii, Uspekhi Fiz. Nauk, 1984, **143**, 329.
66. B.I.Verkin, B.Ya.Sukharevskii, A.I.Gurevich, V.N.Eropkin, and Yu.P.Blagoi, Fiz.Nizkikh Temp., 1984, **10**, 1225.
67. G.P.Singh, H.J.Schink, H.Loneysen, F.Parak, and S.Hunklinger, Z.Phys., 1984, **55**, 23.
68. U.Mizutani and T.B.Massalskii, Nature, 1976, **259**, 505.
69. L.Finegold and J.L.Gude, Nature, 1972, **238**, 33.
70. B.Fanconi and L.Finegold, Science, 1975, **190**, 458.
71. I.-S.Yang and A.C.Anderson, University of Illinois Preprint, ILL-(CM)-87, 1987, p.10.
72. K.V.Shaitan, Vestnik Moskov.Gos.Univ., Fiziki i Astrofizika, 1982, **32**, 15.
73. V.A.Benderskii, V.I.Goldanskii, and A.A.Ovchinnikov, Chem.Phys.Letters, 1980, **73**, 492.
74. L.I.Trakhtenberg and V.N.Flerov, Zhur.Eksper. Teor.Fiz., 1982, **83**, 1908.
75. L.I.Trakhtenberg and V.N.Flerov, Zhur.Eksper. Teor.Fiz., 1983, **85**, 251.

Institute of Chemical Physics,
USSR Academy of Sciences, Moscow